Heliyon 10 (2024) e28275

Contents lists available at ScienceDirect

Heliyon

journal homepage: www.cell.com/heliyon

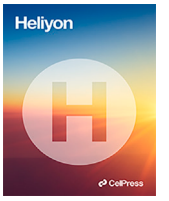

Research article

Band separation and electric field prediction in square Bravais-Moiré photonic crystals

J. Bareño-Silva [a], Á.H. Bedoya-Calle [b,*], H.A. Gómez-Urrea [b], F.J. Caro-Lopera [b]

[a] *Doctorate in Modeling and Scientific Computing, Faculty of Basic Sciences, University of Medellin, Cra. 87 # 30-65, Medellin, 050026, Antioquia, Colombia*

[b] *Faculty of Basic Sciences, University of Medellin, Cra. 87 # 30-65, Medellin, 050026, Antioquia, Colombia*

ARTICLE INFO

Dataset link: https://data.mendeley.com/drafts/7g5ybdxb4k

Keywords:
Bravais-Moiré
Flat bands
Electric field
Riemannian distance
Photonic crystal
Machine learning

ABSTRACT

In this study, we address three key challenges in photonic crystals: modeling of isolated flat bands, electric field prediction, and band separation in dispersion relations. Using twisted square Bravais lattices at specific angles, we create Bravais-Moiré photonic crystals exhibiting unique characteristics. These include band pairing and parallelism in certain Brillouin zones, enabling predictable electric field behavior and identification of isolated, flat band pairs within extensive band gaps. We apply advanced Shape theory-based classification methods for precise band separation, offering significant contributions to photonics research and light manipulation applications.

Acronyms

DFT	Density Functional Theory
GaAs	Gallium Arsenide
PBG	photonic band gap
PCs	Photonic crystals
PQC	Photonic Quantum Computers
QR	QR decomposition
RD	Riemannian distance
SVD	singular value decomposition

1. Introduction

Photonic crystals (PCs) are complex composite structures composed of two or more isotropic media with differing refractive indices and negligible energy losses [1], [2]. These nanostructured materials are engineered to manipulate photon movement, specifically to inhibit and direct the spontaneous emission of light. Independently and simultaneously proposed by [3] and [4], PCs have garnered significant attention for their ability to control light. The design of these materials is such that their dielectric function varies periodically in space, allowing for classification into one-, two-, or three-dimensional structures. The mathematical and physi-

* Corresponding author.
E-mail address: ahbedoya@udemedellin.edu.co (Á.H. Bedoya-Calle).

https://doi.org/10.1016/j.heliyon.2024.e28275
Received 17 July 2023; Received in revised form 28 February 2024; Accepted 14 March 2024

Available online 25 March 2024

cal principles underlying photonic crystals are predominantly analyzed through the Brillouin zone concept. Defined by the primitive cell, the Brillouin zone provides a framework for describing waves propagating in periodic media, using Bloch waves as the basis for this description [5], [6].

Photonic crystals exhibit remarkable properties when subjected to electromagnetic radiation, as evidenced by dispersion relation graphs. These graphs reveal bands that denote allowed modes of propagation within the crystal, which can be flat, semi-flat, or intersecting. Between these bands lie forbidden bands, or band gaps, that prevent the transmission of specific frequencies. The study and classification of these band gaps are of keen interest to researchers due to their potential for diverse applications.

Tunneling through these band gaps is influenced by various factors, including the scatterers' diameter, the materials' refractive index, and the lattice's complexity. A key advancement in the field is the ability to customize these band gaps by altering the crystal's symmetry through defect introduction. This alteration facilitates the occurrence of allowed bands within the gaps, a phenomenon that, coupled with the presence of multiple band gaps and their size variations, represents a significant area for innovative research [7], [8].

In categorizing photonic crystals, factors such as the internal structure's configuration, the geometry, the size of the elements, and the number of components are considered. Central to understanding their properties and aiding in their design is the concept of the unit or primitive cell. This simplest building block allows for the construction of any type of photonic crystal. Through Bravais' classification, specific types of cells, such as square or hexagonal, are identified. Further complexity is achieved by superimposing two rotated Bravais cells, a strategy that leads to intricate lattice structures and is a key focus in the study of twistronics [9].

A subject of particular interest in the study of photonic crystals is the phenomenon of parallel bands. It is crucial to differentiate these from repeated bands, which typically arise when a non-unitary cell is utilized in the analysis. An illustrative example of this issue can be found in the work of [10]. In their study, they attempted to compute the properties of triangular lattices using a standard parallelogram cell but opted instead for a simpler rectangular cell. However, this chosen cell was not the minimal unit, resulting in the duplication of dispersion relations and the overlapping of bands. This highlights the importance of selecting the appropriate unit cell for accurate band representation in photonic crystal analysis

Planar PC has been extensively studied under different geometries, most of them by using the atomic net of the well known five Bravais. Moreover, the twisted graphene studies have emerged into a very popular discipline given the superconductivity properties at magic angles, see for example, [11] and the references therein.

But the paralell study of twistronics in the PC appeared very late. In fact, the mathematical problem in the twistronics has been developed separately according to the required systems (centered and non-centered square, hexagonal, rectangular and oblique). Compare for example the formulae of the hexagonal case in [12], [13], [14]. These discrepancies also need to be solved when an hexagonal Bravais-Moiré PC will be studied.

In recent research, there has been a significant interest in the modeling of minimal commensurabilities and the identification of zones that approximate these models with a high degree of accuracy [15]. This approach is well-documented in the literature by Caro-Lopera (2013) [16], whose notation and methodology we have adopted and elucidated within our methods and results sections. Specifically, the investigation of photonic crystals, particularly the analysis of two twisted square lattices in terms of commensurability, has been thoroughly explored in studies by Gomez-Urrea et al. [17], [18]. In the realm of electronics, the overarching theory has been applied to twisted graphene, as detailed by Tiutiunnyk et al. (2019) [19].

More recently, applications in the study of electronic and magnetic properties of multiple twisted layers have emerged. Leon et al. (2022) presented groundbreaking work in this area. Conceptual framework has led to new insights into the modification of magnetic properties in CrI3CrI3 under commensuration condition [20].

In the photonic crystal (PC) setting, only a few studies have identified unusual behaviors in dispersion relations. To our knowledge, Gomez-Urrea et al. (2020) [18] were the first to document the emergence of band pairs, or permitted modes, both outside and inside the band gaps. These so-called parallel bands, characterized by their flat features, lie very close to each other across one of the three Brillouin zone regions. This behavior, overlooked at the time, now sparks new expectations. In this paper, we aim to elucidate the nature of these parallel bands and their significance in localizing and predicting the field.

The discovery of wide band gaps and parallel bands in one of the three Brillouin zone regions introduces a novel challenge in photonic crystals research. To date, the groundbreaking studies [17] and [18] appear to stand alone in documenting such a distinctive dispersion relation shape. Remarkably, these can be adjusted to produce isolated band pairs that can move within the band gap by manipulating specific parameters, such as the scatterers' radius. This ability enables the creation of wider band gaps with floating flat bands that localize the field within the precisely controlled scatters of the photonic crystal.

The concept of perfect flat bands gives way to the notion of relative flat bands for evaluating band frequency fluctuations as a percentage of the photonic band gap (PBG) that encompasses the band. When this percentage is minimal, approximately 0.5%, the band qualifies as a relative flat band. For instance, the study refered in [21] identified a relative flat band constituting 21% of its corresponding PBG.

With the availability of group theory characterizations for Bravais lattices, as detailed in [22], the understanding of all bands becomes comprehensive, leading to robust applications.

While the complex group theory characterizing Bravais-Moiré patterns remains unsolved, Shape Theory offers a viable alternative for analysis. This emerging field enables the comparison and estimation of average form and variability among objects represented by a set number of landmarks. This rich area of mathematical and statistical study has already shown success across various domains. Traditionally, Shape Theory has been dominated by Gaussian models, as highlighted in works such as those by Goodall and Mardia (1993) [23] and Dryden and Mardia (1998) [24], among others. Subsequently, a more robust framework embracing general models has facilitated stronger applications in scenarios where normal distributions are inadequate. Shape Theory now supports a range of

transformations (including affine, polar, singular value decomposition (SVD), and QR decomposition (QR)) and is applicable to real normed division algebras (such as real, complex, quaternion, and octonion), as demonstrated in studies by [16], [25], [26], [27], [28], [29], [30], [31], [35], [36], [37], [39], [41], [42] and related publications.

This work is distributed as follows: in Section 2.3, we model the dispersion relations in terms of the radius of the cylinders. In particular, we focus on the flattest parallel bands that are characterized from a Riemannian geometry theory useful to quantify the value of the slopes of the bands. Once the flattest pair of bands has been found, it is modeled within the widest gap. In Section 2.4. The electric field prediction is considered for parallel bands in one of the three Brillouin zones. This remarkable aspect is reached by using the invariant Riemannian distance (RD) of shape theory. As an introductory issue, special attention is paid to the calculation of constants corresponding to the location of similar fields in the flat bands. An attempt is made to introduce a new map that relates the field with the frequency with the wave vector, some considerations related to this new map are proposed for future study. Finally, in Section 2.5 we extend the field prediction technique to the remaining two Brillouin zones. The method learns from the RDs in the floating pair in a wide band gap and then it provides a local smooth via for separating the bands.

2. Methods and results

In this section, we present the paper's main findings, which focus on three key areas:

1. Modeling the dispersion relation in parallel bands and floating pair bands of square Bravais-Moiré photonic crystals.
2. Modeling and prediction for the electric field in parallel bands of square Bravais-Moiré photonic crystals.
3. Separation of bands in square Bravais-Moiré photonic crystals.

We base all results on computational analysis using COMSOL software to examine numerous dispersion relations in square Bravais-Moiré photonic crystals. We then analyze, model, and predict the data using Riemannian geometry. The paper details these methods throughout.

Before delving into the three principal contributions of this paper, we outline the test methods and provide an overview of the Bravais-Moiré theory for twisted square layers

2.1. Test methods

We use the Finite Element Method (FEM) to solve Maxwell's equations for photonic crystals with complex geometries. Our strategy involves multi-scale meshing, using finer elements in areas with high field gradients or complex shapes and coarser elements in uniform areas.

Besides calculating field distributions at certain frequencies, we often perform an eigenfrequency analysis. This process solves a generalized eigenvalue problem based on Maxwell's equations, focusing on Transverse Magnetic (TM) mode. In this mode, the electric components lie out of the plane, which is essential for understanding photonic band gaps and slow-light effects.

We employ COMSOL Multiphysics version 5.6 [32], which offers modules tailored for wave optics, using "ewfd" as our solver choice. For post-processing, we develop in-house software [33] use the R programming language [34].

The behavior of electromagnetic waves in photonic crystals is fundamental governed by Maxwell's equations:

$$\nabla \times \mathbf{E} = -\mu \frac{\partial \mathbf{H}}{\partial t} \tag{1}$$

$$\nabla \times \mathbf{H} = \epsilon \frac{\partial \mathbf{E}}{\partial t}$$

The constitutive relations are $\mathbf{D} = \epsilon \mathbf{E}$ and $\mathbf{B} = \mu \mathbf{H}$.

For eigenfrequency analysis, the governing equation is:

$$\nabla \times \mu_r^{-1} (\nabla \times \mathbf{E}) - k_0^2 \left(\epsilon_r - \frac{j\sigma}{\omega \epsilon_0} \right) \tag{2}$$

The wave equation in terms of the electric field $\boldsymbol{E}$ is expressed as

$$\nabla \times \left(\frac{1}{\mu} \nabla \times \boldsymbol{E} \right) - \frac{\omega^2}{c^2} \epsilon \boldsymbol{E} = 0 \tag{3}$$

where k_0 is the free-space wavenumber, $\lambda = -\omega j + \delta$, and the electric field $\mathbf{E}(x, y, z)$ can be represented as $\mathbf{E}(x, y, z) = \overline{\mathbf{E}}(x, y, z)\, e^{-ik} z^z$. For periodic boundary conditions, the equations are:

$$\mathbf{E}_{dst} = \mathbf{E}_{src} e^{-ik_F \cdot (r_{dst} - r_{src})} \tag{4}$$

$$\mathbf{H}_{dst} = \mathbf{H}_{src} e^{-ik_F \cdot (r_{dst} - r_{src})}$$

The refractive index n is given by $n = \sqrt{\epsilon_r}$.

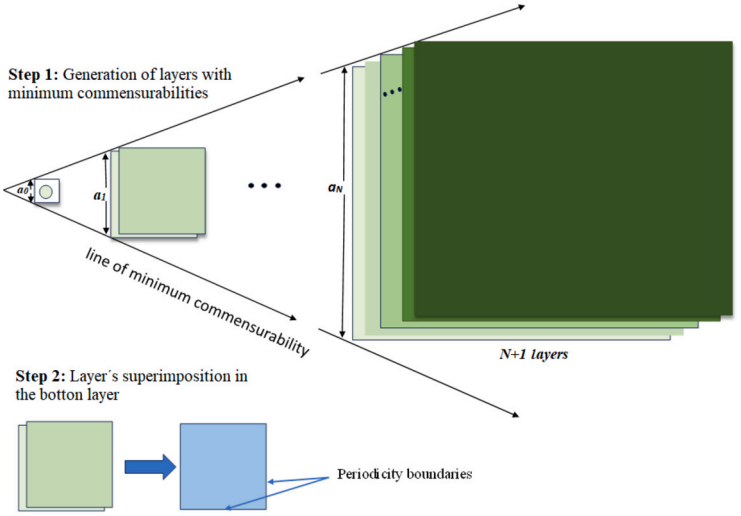

Fig. 1. The scheme outlines the process for creating a two-dimensional photonic crystal. Initially, it involves generating new, commensurate layers using the smallest vector, based on the Caro-Lopera [16] approximation model and concepts from electronic Hamiltonians [15]. This model introduces minor adjustments to the formula for scaling center vectors. The next step illustrates how superimposing the two layers forms a single layer that defines the positions of the dispersers in the two-dimensional photonic crystal.

2.2. Bravais-Moiré square photonic crystals

Two twisted square Bravais under a commensurable angle can be seen as a Bravais-Moire square lattice, where the Moiré patterns appear in a periodic way. The usual unit square cell of one scatter can be used for replicating the complete twisted lattice under the concept of atomic net.

Our implementation in twisted Bravais emerges in the context of commensurable multilayer rotated affine latices studied by [16]. This approach for n layers and multiple Bravais, has been published in certain two dimensional and bilayers Bravais, see [38], [19], [17], [18], [40]. This has been applied by first time in twisted magnetic systems, transcending the usual twistronic studies, see [20]. Emerging other works with similar approach and simplifications like Kariyado & Vishwanath, (2019) [15] that presented a minimum commensurable angles in the Density Functional Theory (DFT) electronic uses. We show in Fig. 1 a general scheme for the generation of two-dimensional PCs from these approaches and the reader can see in detail from this section.

The square Bravais-Moiré theory is presented next for twisted bilayer of cylinders projected into a two dimensional plane forming a two dimensional photonic crystal.

Consider the $k\frac{\sqrt{2}}{2}Z \times k\frac{\sqrt{2}}{2}Z$ lattice, where k is a constant usually imposed when the discrete set of points is seen as a crystallographic atomic structure; for example, $k = 1.44$Å is taken for hexagonal Bravais lattice of graphene.

There a number of possible primitive vectors that span the lattice, in particular, we propose the following:

$$\mathbf{u}_1 = k\sqrt{2}\begin{pmatrix} 1 \\ 0 \end{pmatrix}$$
$$\mathbf{u}_2 = k\sqrt{2}\begin{pmatrix} 0 \\ 1 \end{pmatrix} \tag{5}$$

As usual, Moiré patterns appear when a second Bravais lattice, B_{rot}, initially coincident with B_{norot}, is rotated, around the same reference center, by certain angle θ. The rotation θ is defined as a commensurable angle if the vector position $\mathbf{c}_{r,s}$, for a pair of integers r and s of B_{norot} coincides with the vector position $\mathbf{c}_{r',s'}$, for a pair of integers r' and s' of B_{rot}.

Under a commensurable rotation θ, the symmetry of the resulting Moire patterns divides the plane in eight equal parts: $0 < \theta < \pi/4$, $\pi/4 < \theta < 2\pi/4$, ..., $7\pi/4 < \theta < 8\pi/4$, numbered counterclockwise. So, in terms of the non rotated reference system, the primitive vertices are located at:

$$p_1 = \left(\sqrt{2}r, \sqrt{2}s\right)$$
$$p_2 = \left(-\sqrt{2}s, \sqrt{2}r\right)$$
$$p_3 = \left(-\sqrt{2}r, -\sqrt{2}s\right)$$
$$p_4 = \left(\sqrt{2}s, -\sqrt{2}r\right), \tag{6}$$

where the associated commensurable angle $0 < \theta < \frac{\pi}{2}$ is given by:

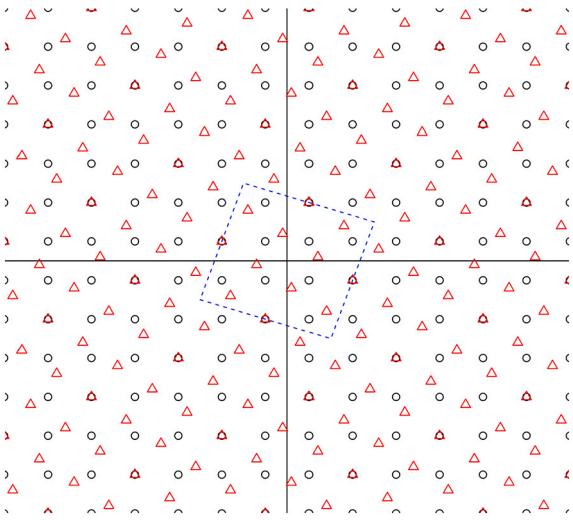

Fig. 2. Super square Bravais-Moiré unit cell associated with $(r = 2, s = 1)$ and superimposition of first lattice (circles) and second lattice (triangles) with a commensurable rotation 36.9°.

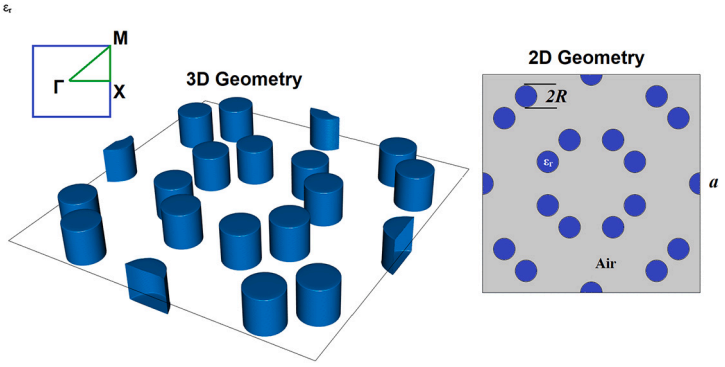

Fig. 3. Commensurable square Bravais−Moiré unit cell (a) associated with $(r = 2, s = 1)$. The Brillouin zone defines a piecewise function for k_x and k_y based on k, which changes along the path from Γ to X to M and back to Γ. In the segment from Γ to X, for $0 \leq k \leq 1$, k_x increases linearly from 0 to π/a with k, and k_y stays at zero, showing movement along the x-axis in reciprocal space. From X to M, as k moves from 1 to 2, k_x remains constant at π/a, and k_y increases linearly from 0 to π/a, indicating diagonal path towards the M point. Lastly, on the way back from M to Γ, both k_x and k_y linearly decrease from π/a to 0 as k changes from 2 to 3, finishing the way at starting point. This piecewise formulation effectively maps the path taken through symmetry points in the Brillouin zone.

$$\theta = \cos^{-1}\left(\frac{2rs}{r^2+s^2}\right), r, s \text{ coprimes}, r > 1,\ s > 0,\ r > s. \tag{7}$$

The primitive vertices form a super square cell which is useful for studying some additional geometrical properties of commensuration and non-commensuration.

In DFT, the Bravais-Moiré commensurable cell is three-dimensional and two layers B_{norot} and B_{norot} are separated according to the electronic interaction laws. We can form a similar three dimensional photonic crystal with both layers, but in this paper we superimposed B_{norot} and B_{norot} in order to construct a two dimensional crystal.

Each pair of parameters r and s defines rich super commensurable unit cell for research, however, we will focus in the simplest square Bravais-Moiré indexed by $r = 2, s = 1$. in this Bravais-Moiré the number of points for the commensurable square cell is given by

$$N = 4(r^2 + s^2) + 4, \qquad r = \frac{m+n}{2},\ s = \frac{n-m}{2},\ m, n = 1, 3, 5, 7, \ldots; m < n. \tag{8}$$

Here m, n are selected in such a way that the resulting r, s are coprimes and $r > 1, s > 0, r > s$.

We consider the simplest square Bravais-Moiré indexed by $r = 2, s = 1$; the complete super square commensurable cell after imposition of two rotated Bravais by 36.9° is depicted in Fig. 2. The corresponding unit cell under commensurability is shown in Fig. 3.

2.3. Modeling the dispersion relation in parallel bands and floating pair bands of square Bravais-Moiré photonic crystals

Now we are in position to study the first problem of the paper.

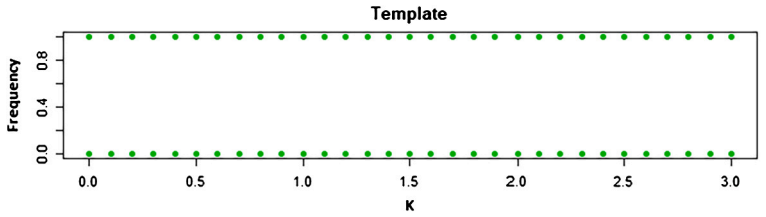

Fig. 4. Template of a difference for a perfect parallel pair.

For practical purposes for the models, We will be focus on the $X - M : 1 \leq k \leq 2$ where the parallel pair of bands occur.

In the corresponding dispersion relations an interesting and very rare feature is noticed: one of the three Brillouin zones joins the bands by pairs. The bands are extremely near and parallel. Modeling and predicting that unusual behavior will be the goal of this section.

As can see in Fig. 3 materials based on Gallium Arsenide (GaAs) with real dielectric constant $\epsilon_r = 12.9$ are used as material for the scatters (blue), and air as background. We start with the dispersion relation of 37 radios $R = p.a$ for the scatters, ranged from $p = 0.026$ to $p = 0.0688$ with step 0.00119. Here, $a = 13.01451442\mu m$ is the lattice constant of the square commensurable cell indexed by $r = 2$ and $s = 1$ of the Bravais-Moiré. The evolution of 30 bands associated with each radius is shown in the animated Figure S3 of the Supplementary material. Note the 15 joined and parallel pairs in the zone defined by $k = 1.0$ to $k = 2.0$. This property is constant for all the 37 radios under consideration and every Bravais-Moiré indexed by every suitable parameter r and s ($r > s$ coprimes, $r >= 2$, $s >= 1$).

Throughout the paper we will number the bands according to the classification given by COMSOL. The data provided by the software orders the bands according to non expert classification of the light path, it just defines the most horizontal possible path for a neighborhood of the frequency. Then it colors the bands and gives 30 matrices with the corresponding k and frequency. It is easy to see that the COMSOL classification do not reach a plausible band, because it breaks the required differentiability when the paths are crossed each other, however, we will use that classification for developing our method. Thus, until a realistic classification is given at the end of the paper, we will understand the bands as those colored by COMSOL.

We now restrict the analysis to the extreme near pairs of bands in the zone defined by $k = 1.0$ to $k = 2.0$, in the scale of the complete zone for k the seems one, in fact if we zoom it the difference is so small. First we note the parallelism of each band by drawing the difference of the upper and the lower band of each pair. The animated Figure S4 of the Supplementary Material shows the difference of the frequencies for all the 15 pairs in the zone $k = 1.0$ to $k = 2.0$.

Now, we search for the best parallel pair, which is given for horizontal lines for all the radios. A way for selection can be drawn from a recent method of classification called shape theory. A perfect template in this case is given for two parallel bands, the lower one at frequency 0 and the upper line at frequency 1, see Fig. 4. If this template is compared with a perfect parallel pair of bands, the RD between both pairs are just 0. Once the discrepancy is increased, the Riemannian distance also aparts from 0 until the maximal distance is reached at $\pi/2$. The RD will describe deeply in the following section. At this time we just want to provide a simple punctuation of the similarity or dissimilarity of a given pair of colored bands by COMSOL.

Once we found all the RDs between the template and each pair for all the radios, we compute the mean of the corresponding 37 measures. The results are shown in Fig. 4 of the Supplementary Material.

Then automatic detection provides the pair 9 of bands 17 and 18 as the best parallel bands in the zone $k = 1.0$ to $k = 2.0$. This pair is also the floating band that we referred before, which is moving throughout a wide band gap.

We now focus our attention in such interesting pair. The RD of a template and each difference of the pair 9 in terms of the 37 radios is given in the Fig. 5.

In this case the best parallel pair is obtained for the greater radius associated with $p = 0.0688$.

Fig. 6 shows the total field accumulation in the cylinders respect to the bands.

Note that the highlighted pair 9 (black spots) shows the maximum field accumulation in all the cylinders. In this case the unit corresponds to the pixels under a heat camera color of the field, given by COMSOL. Under this parameterization, the total content of the field is just the total number of pixels.

We can try a so-called photonic constant map in order to find a possible relation between the accumulated field in the cylinders and a corresponding frequency, see Fig. 7.

Observe that the best constant is reached in the pair 9 (red spots). For getting this end, we compute theRDs for all curves in contrast with the perfect template. In this case is given for two parallel lines, the lower one at constant 0 and the upper line at constant 1, see Fig. 4.

Finally, we can check the evolution of the constant in terms of the bands, see Fig. 8.

Note that the constant is stabilized by high frequencies. The clarification of this new topic of research for a constant in photonic crystals is studied by the authors.

However, a most significant and notorious aspect can be research in the square Bravais-Moiré. We will detail it in the next section.

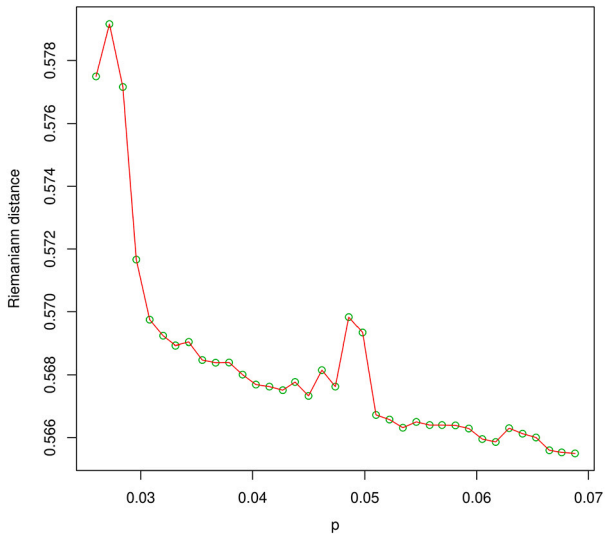

Fig. 5. Evolution of the parallelism of pair 9 in terms of the $r = p.a$, where $a = 13.01451442\mu m$ is the lattice constant and p ranges from $p = 0.026$ to $p = 0.0688$ with step 0.00119.

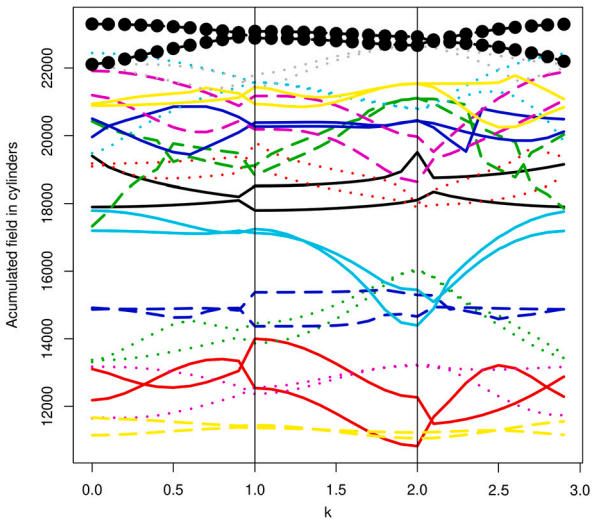

Fig. 6. Total accumulation of the electric field (TM mode) in the cylinders with respect to the bands.

2.4. Modeling and prediction for the electric field in parallel bands of square Bravais-Moiré photonic crystals

In this section we provide a way of predicting the field in parallel bands of square Bravais-Moiré photonic crystals. Then it promotes a general method for separating pairs of bands in the corresponding dispersion relation.

Start with the floating pair of bands 17 and 18. Fig. 9b shows the electric field for $k = 1.5$ of band 17. The superior band 18 of the pair in the same $k = 1.5$ is given in Fig. 9a.

The strong symmetry of both fields, concentrated in the cylinders, seem to be related each other. However, consider the pair of bands 5 and 6, with non-symmetric field of Figs. 10b and 10a, then we ask for a possible relation too.

Similar pictures can be shown in the Brillouin zone defined by $1.0 \leq k \leq 2.0$, where the parallelism is evident between ordered pair bands, 1-2,3-4,...,17-18,...,29-30. Now, we ask for a relationship between the field of the inferior and superior band of each pair of bands in the referred $1.0 \leq k \leq 2.0$.

For the bands 17 and 18 of Fig. 9 we have the following simple composition of Fig. 11, which can be seen as a prediction of the field for superior band, by using the field in the inferior parallel band.

In a similar way, we can predict the Electric field of band 6 by using the field of band 5, at $k = 1.5$. See Fig. 12.

We have obtained the same interesting predictions of the superior band with the inferior band for every pair (1 to 15) of parallel bands and for each $k = 1.0, 1.1, ..., 2.0$. The animated Figure S3 of the Supplementary Material shows the prediction for all the 15 pairs under consideration.

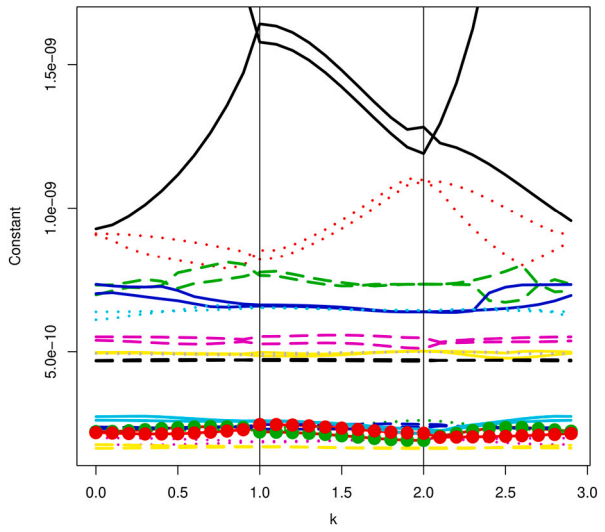

Fig. 7. Photonic constant map for the relation of cummulative field and frequency, for all bands.

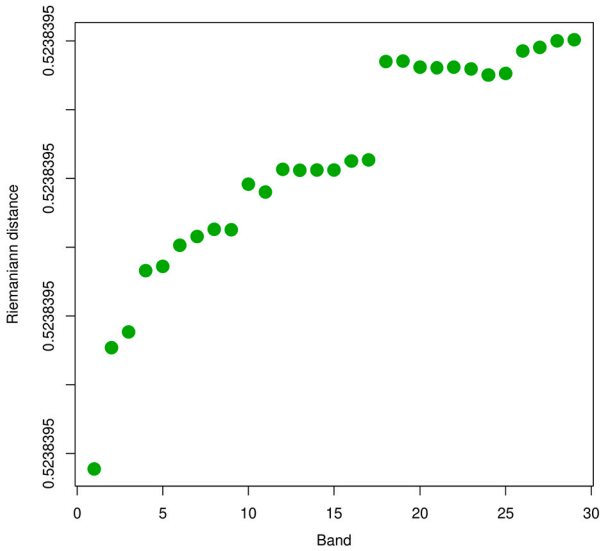

Fig. 8. Evolution of the constant in terms of the bands. Numerical y-axis value present here differs from the 9th decimal, so it is not possible to differentiate it and they are very close.

Moreover, this field behavior is repeated in all the square Bravais-Moiré that we have studied. For example, for the photonic crystal indexed by $r = 3, s = 1$ the band 13 predicts the field of band 14 at $k = 1.5$, according to the Fig. 13.

Until now, the group characterization theory of the Bravais-Moiré photonic crystal is far to be discovered; then we need to provide a mathematical way of proving the addressed prediction in the parallel bands.

For getting this end, instead of the composition given in Figs. 9, 10, 13 we just consider a change of the periodic conditions in the unitary cell, which perform the same prediction.

The procedure is depicted in Fig. 14

We divide in four equal quadrants the unitary field cell of the inferior band. Then the periodic propagation or prediction for the field of the superior band switch the quadrant 2 (ABCD) with quadrant 4 (A'B'C'D'); in the same way that quadrant 1 (EFGH) changes the position with quadrant 3 (E'F'G'H'). For a proof that both fields are near for the parallel band in the Brillouin zone $1.0 \leq k \leq 2.0$, we apply the addressed recent mathematical theory of classification based on Riemannian geometry. Among other functionalities, Shape theory considers the equality or dissimilarity of objects summarized by matrices in certain quotient spaces fibered by a number of transformations. In particular, let $Q_i, i = 1, 2, 3, 4$ be an $n \times 3$ matrix collecting the field and coordinates of the i-th quadrant. The first and second columns provide the x, y coordinates of the n pixels and the corresponding field are given in the third column.

The shape of the three dimensional field of the i-th quadrant attains all geometrical information that remains after filtering out the location, scale and rotation from Q_i.

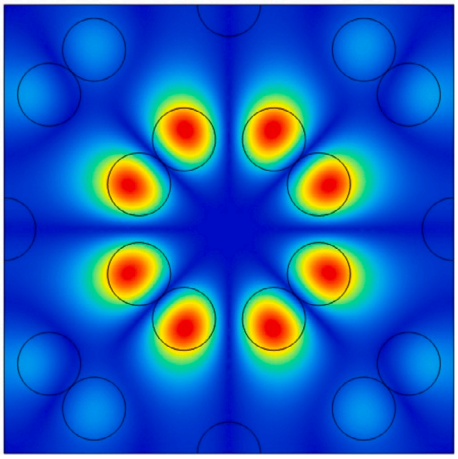

(a) Field of band 18 at $k = 1.5$

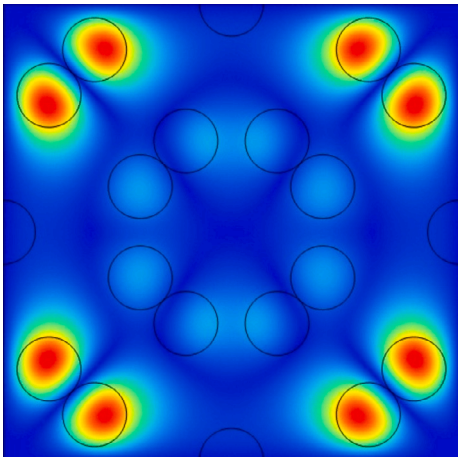

(b) Field of band 17 at $k = 1.5$

Fig. 9. Electric field for the parallel bands 17 and 18.

In that sense, the invariant location and scaling, so-called pre-shape matrix P_{Q_i} can be seen as a point in a unitary hypersphere in $3(N-1)$ real dimensions, then the shape of a given quadrant Q_i is the set of all coincident pre-shapes quotiented by rotation on a great circle with P_{Q_i}. With this principle, we can define a distance between two quadrants Q_i, Q_j by using the RD. This can be seen as an angle ranged from 0 (perfect similarity) to $\pi/2$ (maximal dissimilarity), which is the closest distance in the great circle of two preshapes in the hypersphere. The expression for RD is given as follows:

$$RD(Q_i, Q_j) = \arccos \sum_{t=1}^{3} b_t \tag{9}$$

where b_t are the square roots of the eigenvalues of $B'_f B_g B'_g B_f$. $B_p = \frac{1}{U_p} C N_p$, $p = f, g$; $U_p = \sqrt{\text{trace}\{[EN_p]'[EN_p]\}}$, $p = f, g$; $E = \left(I_n - \frac{1}{n} 1_n 1'_n\right)$, I_n is the identity matrix, 1 is a vector of ones, $'$ is the matrix transpose. $C = (c_i)$ is a $(n-1) \times n$ matrix such that

$$c_i = \left(\underbrace{-\frac{1}{\sqrt{i(i+1)}}, ..., -\frac{1}{\sqrt{i(i+1)}}}_{i}, \frac{i}{\sqrt{i(i+1)}}, 0, ..., 0 \right).$$

First, we focus on the parallel zone defined by $k = 1.0, ..., k = 2.0$. The bands are not classified in the sense that they are just colored by a horizontal neighborhood given in COMSOL, thus the current definition for bands 1 to 30 does not correspond to the real bands tracing the light path in the photonic crystal. The bands colored by COMSOL are not differentiable paths, as we expect from the solution of Maxwell's equations. Separating the bands with smooth criteria is the biggest challenge of the paper. We start by explaining the parallelism of the band pairs in the middle Brillouin zone, in terms of the field.

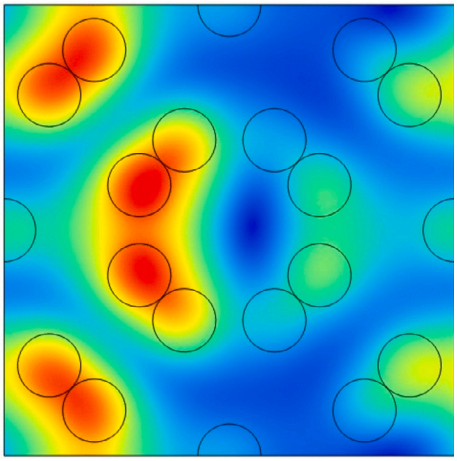

(a) Field of band 6 at $k = 1.5$

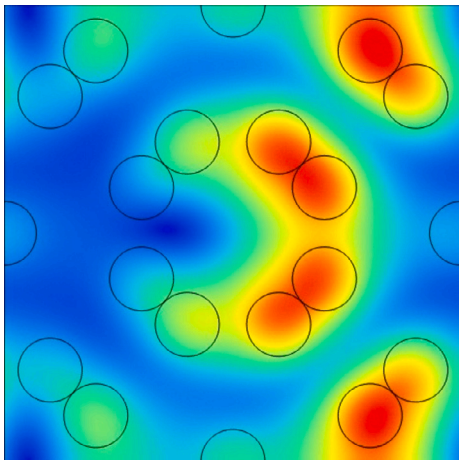

(b) Field of band 5 at $k = 1.5$

Fig. 10. Electric field for the parallel bands 5 and 6.

For a robust method, we need to learn from the data by computing all the possible RDs among the four quadrants of every combination of bands in the Brillouin zone parameterized by $k = 1.0, ..., 2.0$. The exhaustive computation can be seen in Tables S7 to S50 of the Supplementary Material.

In all the tables, the RD is extremely sensitive for dissimilar fields in non-paired and consecutive bands. The numerical proof that we are searching for appears in the diagonal of each Table S7 to S50. They explain the similarity of the given quadrant of the inferior band with the expected prediction on the corresponding quadrant in the superior band.

For example, if we extract the required information for $k = 1.5$ we find the following uniform distribution of RD, very near to zero, for the expected 15 pairs. See Table 1 and Table S136 in SI.

Similar behavior can be seen in the remaining $k = 1.0, ..., 2.0$. We have separated the diagonal values in Tables S131 to S141 of the Supplementary Material.

Note the remarkable low RD in all the quadrants and pairs, a fact that shows the parallelism between the bands in such Brillouin zone. Observe also the verification of the periodic switchable condition via the strong symmetry in the RD of Q_1Q_3 and Q_3Q_1, and Q_2Q_4 and Q_4Q_2.

This interesting behavior applies now for a field prediction in the middle Brillouin zone of other parameterized Bravais-Moiré with the integers r and s, see again Fig. 13 and [18], [17].

Meanwhile the claimed and difficult open problem for a group theory characterization of Bravais-Moiré photonic crystals is solved, we consider the proposed method based on RD as a sufficient proof for such splendid behavior of the pairs in the Brillouin zone defined by $1.0 \leq k \leq 2.0$.

2.5. Separation of bands in square Bravais-Moiré photonic crystals

Start with the dispersion relation of the first 30 normalized bands given by COMSOL, see Fig. 15. The scale in the frequency has units $\frac{\omega a}{2\pi c}$, with c the speed of light in the vacuum.

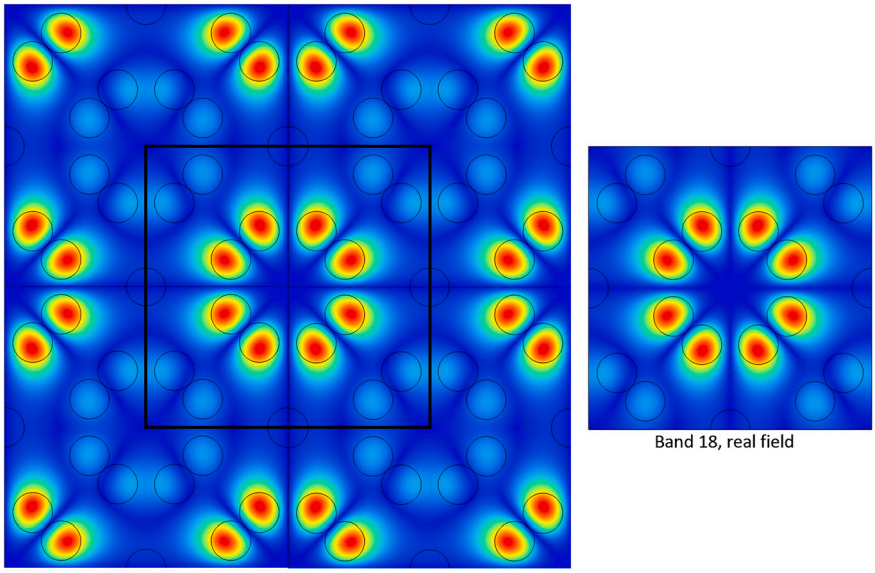

Fig. 11. Prediction of the Electric field of band 18 by using the field of band 17, at $k = 1.5$.

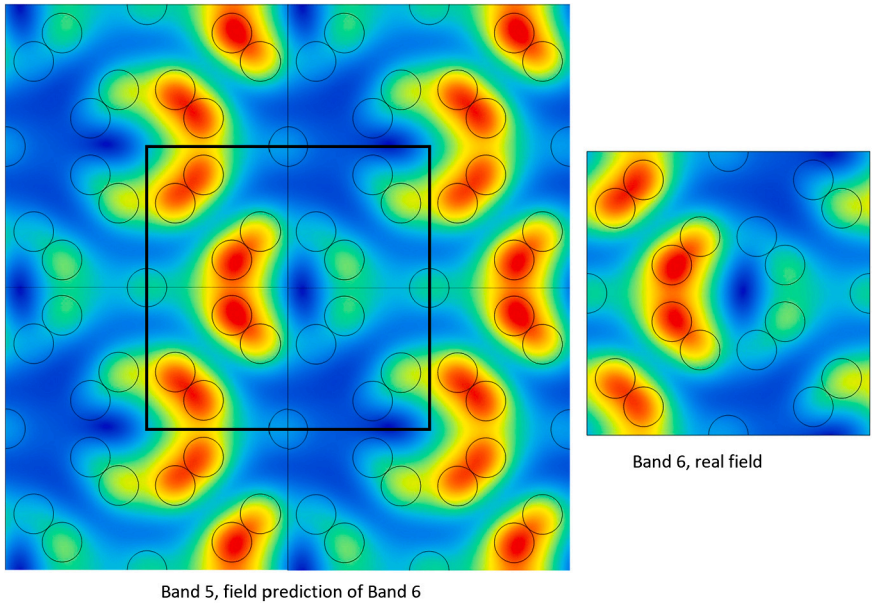

Fig. 12. Prediction of the Electric field of band 6 by using the field of band 5, at $k = 1.5$.

It should be noted that the colored separation is not realistic because the expected differentiability of any path is broken, then a method for suitable isolation of the bands is claimed.

The separation of bands in any dispersion relation of light (or electrons) in photonic crystals (or materials) is one of the major challenges in physics. Excepting, trivial systems of one scatter in square or hexagonal photonic crystals, the intricate path of light is so difficult to elucidate. In systems of several scatters, the dispersion relations just show all the band in only one color, without any separation of the specific path followed by each band.

However, in the previous Section, we noted that the bands in certain Brillouin zone are strictly parallel with a remarkable order, allowing an accurate prediction of the field. Then the preceding apart can promote a general method for separating pairs of bands in the dispersion relations of Bravais-Moiré photonic crystals. If the bands are tied by pairs in the Brillouin zone defined by $1.0 \leq k \leq 2.0$, then according to the continuously differentiable solutions of Maxwell's equations they must be tied too in the remaining Brillouin zone defined by $0.0 \leq k < 1.0$ and $2.0 < k \leq 3.0$. The dispersion relations do not exhibit parallelism in those zones, then the field is not closely predicted. But the continuous differentiability guarantees a smoothness change of the field. And it should be related to

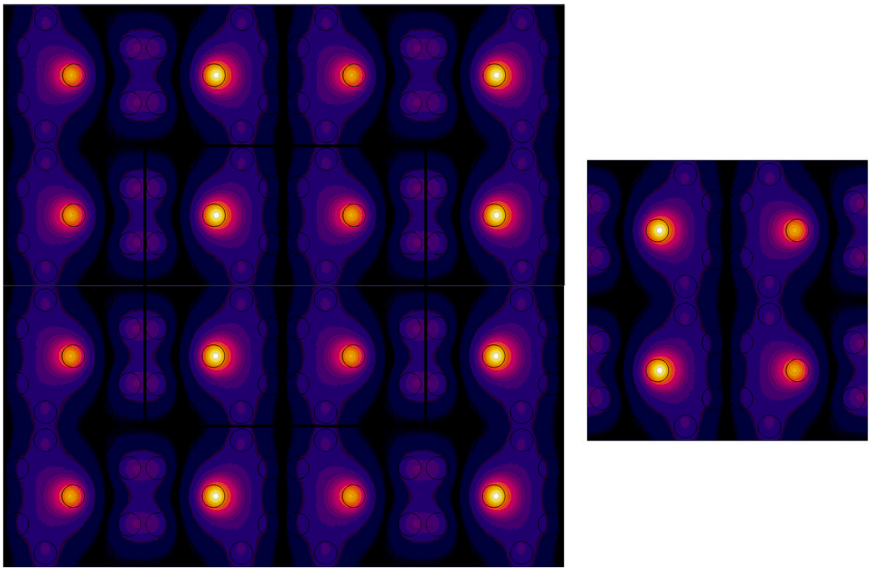

Fig. 13. Prediction of the Electric field of band 14 by using the field of band 13 ($k = 1.5$) for a Bravais-Moiré photonic crystal parametrized by $r = 3, s = 1$.

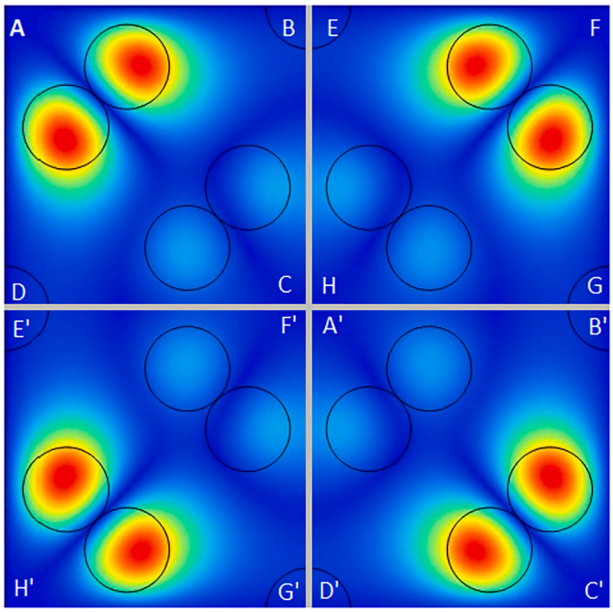

Fig. 14. Change of the periodic conditions for the field of the inferior band in order to predict the field of the superior band for a given pair of parallel bands at $1.0 \leq k \leq 2.0$.

small Riemannian distances of quadrants; according to the change of the proposed periodic conditions for the superior band in terms of the inferior band of the pair. See again Fig. 14.

Again the method just learns from all possible combinations of quadrants and pairs. For the Brillouin zone parameterized by $0.0 \leq k < 1.0$, see Tables S51 to S90 in the Supplementary Material. When $2.0 < k \leq 3.0$, the corresponding combinations are given in Tables S91 to S130 of the Supplementary Material. The RDs are again computed under the original and nonexpert classification provided by COMSOL in a horizontal neighborhood of the band propagation. In this case, the diagonal of the Tables does not provide a realistic and expected behavior because the colored bands cross each other in non-differentiable paths. This fact is noted by the RD. When we separate the diagonals we note a drastic change in the Rd, see Tables S152 to S161 and S142 to S151 in the Supplementary Material. Then we cannot infer the path of each pair by using the addressed diagonals, but we can extract the right propagation by following the smooth changes in the RD in other regions of the complete Tables S51 to S90 and S91 to S130 of Supplementary Material.

For this colossal task we learn from an isolated and exceptional pair of bands which we have modeled in the firts part of this work. The isolated and floating bands 17 and 18 immersed in a wide band gap are the key for this learning machine via RD. Bands

Table 1
RD of the 15 band pairs at $k = 1.5$.

B_{inf}	B_{sup}	Q_1Q_3	Q_3Q_1	Q_2Q_4	Q_4Q_2
1	2	0.02	0.02	0.02	0.02
3	4	0.01	0.01	0.01	0.01
5	6	0.02	0.02	0.02	0.01
7	8	0.01	0.01	0.01	0.01
9	10	0.01	0.01	0.01	0.01
11	12	0.01	0.01	0.02	0.02
13	14	0.01	0.01	0.01	0.01
15	16	0.01	0.01	0.01	0.01
17	18	0.01	0.01	0.01	0.01
19	20	0.01	0.01	0.01	0.01
21	22	0.02	0.02	0.02	0.02
23	24	0.02	0.02	0.02	0.02
25	26	0.02	0.02	0.02	0.02
27	28	0.02	0.02	0.02	0.02
29	30	0.02	0.02	0.02	0.02

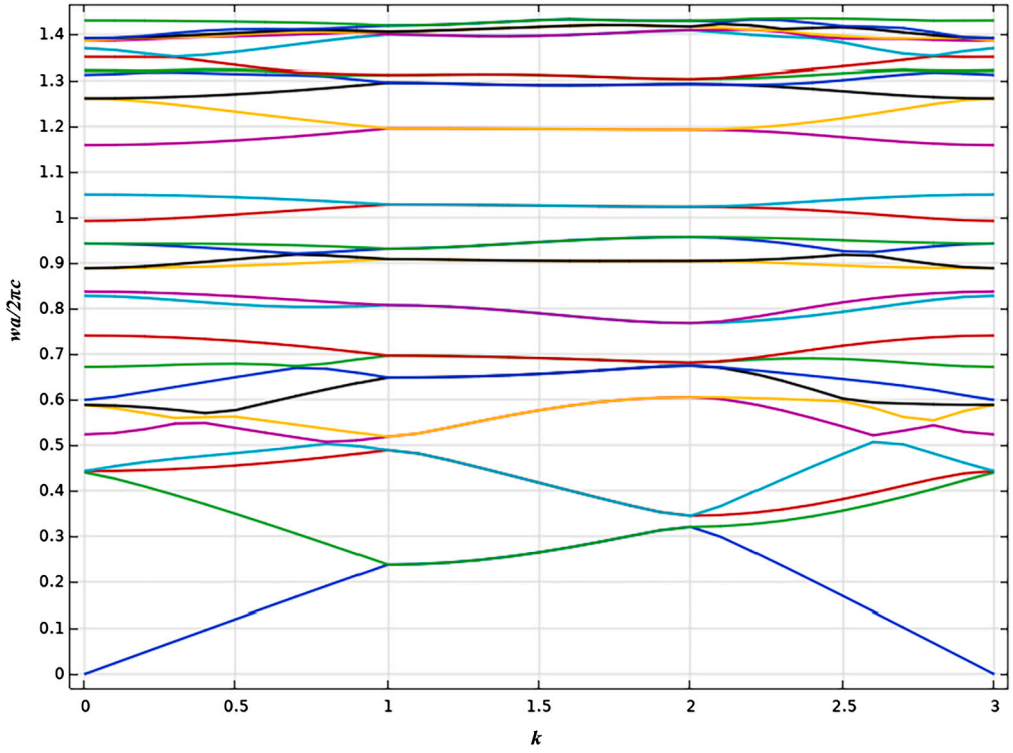

Fig. 15. Dispersion relation of the first 30 normalized bands colored by COMSOL using a horizontal neighborhood.

17 and 18 are exceptional because they are also relatively flat in the Brillouin zone defined by $1.0 \leq k \leq 2.0$; thus it concentrates the field inside the scatters. This remarkable property is useful for posterior transmission applications and fabrication of the photonic crystal. As far we have experimented, all the studied square Bravais-Moiré had an isolated, floating, and relatively flat pair, then the proposed method for band differentiation can be explored.

In this isolated pair 17-18, the corresponding 9-th row of Tables 152 to 161 and 142 to 151 of Supplementary Material do show the real deviation of the RD due to the non parallelism and non-crossing with other bands. We have collected the results in the following Table 2.

Note that the RD is consistently held low in at least two pairs of quadrants in the complex zones $0.0 \leq k < 1.0$ and $2.0 < k \leq 3.0$.

For the correctness of classification method inherited from the isolated and floating bands, we collect the RD for the 6th pair of bands 11 and 12. The results are given in Table 3.

Again the pattern in first ($0.0 \leq k < 1.0$) and third ($2.0 < k \leq 3.0$) parameterized Brillouin zone is held, with at least two quadrants of low RD. This pair of bands 11 and 12 shows a non-well localized field in the cylinders, thus it is not suitable for posterior transmission and fabrication of photonic crystal. However, it is crucial for training the method of classification for crossing bands, because it lies in a wide band gap.

Table 2
RD of the isolated and floating 9th pair of bands 17 and 18 for all k.

k	Q_1Q_3	Q_3Q_1	Q_2Q_4	Q_4Q_2
0.0	0.08	0.08	0.10	0.09
0.1	0.09	0.09	0.09	0.08
0.2	0.09	0.09	0.09	0.08
0.3	0.09	0.09	0.09	0.09
0.4	0.09	0.09	0.09	0.09
0.5	0.09	0.09	0.09	0.09
0.6	0.09	0.09	0.09	0.09
0.7	0.03	0.03	0.03	0.03
0.8	0.03	0.03	0.03	0.03
0.9	0.02	0.02	0.02	0.02
1.0	0.01	0.01	0.01	0.01
1.1	0.01	0.01	0.01	0.01
1.2	0.01	0.01	0.01	0.01
1.3	0.01	0.01	0.01	0.01
1.4	0.01	0.01	0.01	0.01
1.5	0.01	0.01	0.01	0.01
1.6	0.01	0.01	0.01	0.01
1.7	0.01	0.01	0.01	0.01
1.8	0.01	0.01	0.01	0.01
1.9	0.01	0.01	0.01	0.01
2.0	0.02	0.02	0.04	0.04
2.1	0.67	0.68	0.07	0.07
2.2	0.64	0.65	0.06	0.06
2.3	0.62	0.62	0.05	0.05
2.4	0.60	0.60	0.05	0.04
2.5	0.58	0.59	0.04	0.04
2.6	0.71	0.71	0.15	0.16
2.7	0.73	0.73	0.11	0.11
2.8	0.75	0.75	0.09	0.09
2.9	0.77	0.77	0.08	0.08
3.0	0.08	0.08	0.10	0.09

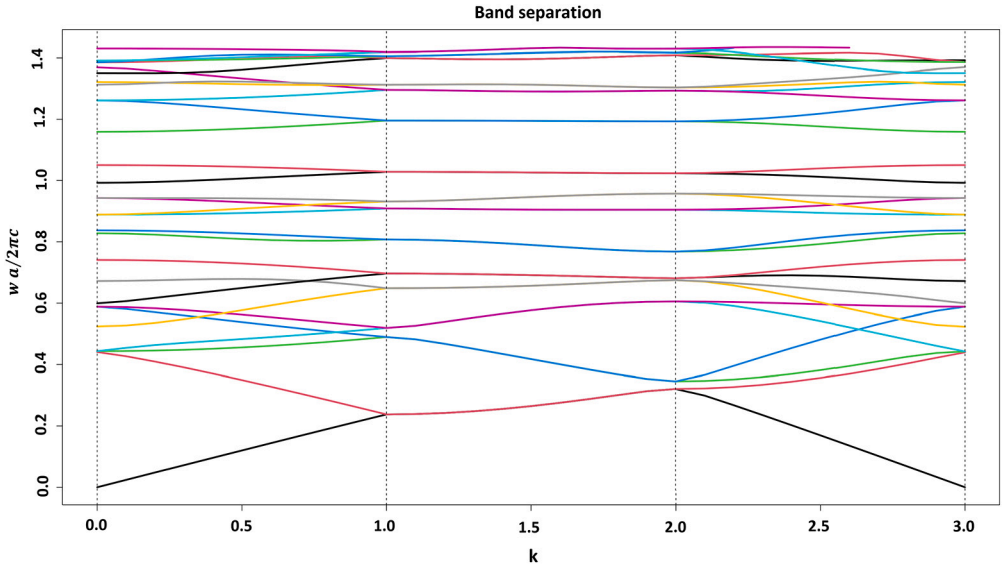

Fig. 16. Realistic dispersion relation of the first 30 normalized bands separated by the Riemannian geometry method.

Once we have trained the expected differences in RDs we search for local smoothness of variation of RD in the other bands, which are not inside a band gap. After a careful analysis of consecutive bands in Tables S51 to S90 and S91 to S130 of the Supplementary Material, we finally provide the correct separation of the pairs. Each pair is depicted in the following Tables 4, 5 and 6.

The real bands 28 and 30 are incomplete because COMSOL does not separate the bands, and just brings 30 colored bands in a neighborhood of the frequencies. The remaining paths of the isolated bands must be found in upper frequencies.

Finally, we obtain the dispersion relation with the separated real bands, see Fig. 16.

Table 3
RD of the isolated and floating 6-th pair of bands 11 and 12 for all k.

k	Q_1Q_3	Q_3Q_1	Q_2Q_4	Q_4Q_2
0.0	0.14	0.14	0.14	0.14
0.1	0.14	0.14	0.14	0.14
0.2	0.14	0.14	0.14	0.14
0.3	0.15	0.15	0.15	0.15
0.4	0.15	0.15	0.15	0.15
0.5	0.14	0.14	0.14	0.14
0.6	0.12	0.12	0.12	0.12
0.7	0.09	0.09	0.09	0.09
0.8	0.06	0.06	0.06	0.06
0.9	0.03	0.04	0.04	0.03
1.0	0.01	0.01	0.01	0.01
1.1	0.01	0.01	0.01	0.01
1.2	0.01	0.01	0.01	0.01
1.3	0.01	0.01	0.02	0.02
1.4	0.02	0.01	0.02	0.02
1.5	0.01	0.01	0.02	0.02
1.6	0.02	0.02	0.02	0.02
1.7	0.02	0.02	0.02	0.02
1.8	0.02	0.02	0.02	0.02
1.9	0.02	0.02	0.02	0.02
2.0	0.02	0.02	0.02	0.02
2.1	0.24	0.24	0.12	0.12
2.2	0.31	0.31	0.17	0.18
2.3	0.36	0.36	0.16	0.17
2.4	0.34	0.34	0.15	0.15
2.5	0.30	0.31	0.13	0.13
2.6	0.26	0.26	0.10	0.10
2.7	0.22	0.22	0.08	0.08
2.8	0.18	0.18	0.08	0.08
2.9	0.15	0.16	0.12	0.11
3.0	0.14	0.14	0.14	0.14

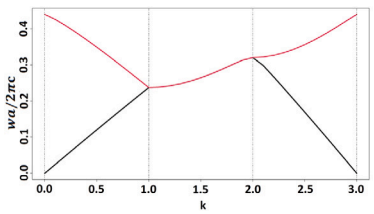

(a) Isolated pair 1 of degree 1 with separated bands 1 and 2

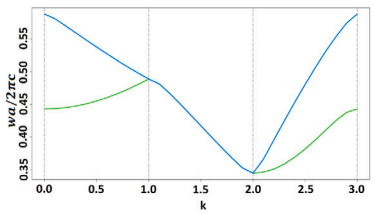

(b) Isolated pair 2 of degree 1 with separated bands 3 and 4

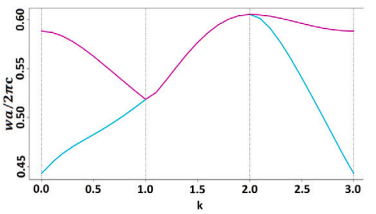

(c) Isolated pair 3 of degree 1 with separated bands 5 and 6

Fig. 17. Separated bands of pairs 1, 2, 3.

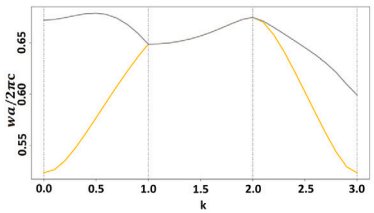

(a) Isolated pair 4 of degree 2 with separated bands 7 and 8

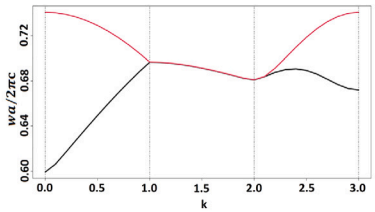

(b) Isolated pair 5 of degree 2 with separated bands 9 and 10

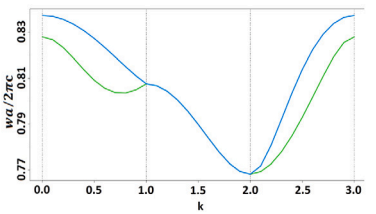

(c) Isolated pair 6 of degree 1 with separated bands 11 and 12

Fig. 18. Separated bands of pairs 4, 5, 6.

In Figs. 17a to 21c we illustrate the separated pairs.

We will call pairs of order 1 to those simple duets of bands coincident in $k = 0,0$ and $k = 3.0$. They can be seen as two closed independent paths which do not cross each other and form a perfect loop. The order counts the number of joining bands required for completing a perfect loop in $k = 0,0$ and $k = 3.0$ The pairs 1, 2, 3, 6, 7, 8, 9, 10 are of order 1, see Figs. 17a, 17b, 17c, 18c, 19a, 19b, 19c, 20a.

Table 4
Separation of bands in terms of the original colored bands of COMSOL. Bands 1 to 10.

k	B_1	B_2	B_3	B_4	B_5	B_6	B_7	B_8	B_9	B_{10}
0.0	1	2	3	6	4	7	5	9	8	10
0.1	1	2	3	6	4	7	5	9	8	10
0.2	1	2	3	6	4	7	5	9	8	10
0.3	1	2	3	6	4	7	5	9	8	10
0.4	1	2	3	5	4	7	6	9	8	10
0.5	1	2	3	5	4	6	7	9	8	10
0.6	1	2	3	5	4	6	7	9	8	10
0.7	1	2	3	5	4	6	7	9	8	10
0.8	1	2	3	5	4	6	7	8	9	10
0.9	1	2	3	4	5	6	7	8	9	10
1.0	1	2	3	4	5	6	7	8	9	10
1.1	1	2	3	4	5	6	7	8	9	10
1.2	1	2	3	4	5	6	7	8	9	10
1.3	1	2	3	4	5	6	7	8	9	10
1.4	1	2	3	4	5	6	7	8	9	10
1.5	1	2	3	4	5	6	7	8	9	10
1.6	1	2	3	4	5	6	7	8	9	10
1.7	1	2	3	4	5	6	7	8	9	10
1.8	1	2	3	4	5	6	7	8	9	10
1.9	1	2	3	4	5	6	7	8	9	10
2.0	1	2	3	4	5	6	7	8	9	10
2.1	1	2	3	4	5	6	7	8	9	10
2.2	1	2	3	4	5	6	7	8	9	10
2.3	1	2	3	4	5	6	7	8	9	10
2.4	1	2	3	4	5	6	7	8	9	10
2.5	1	2	3	4	5	6	7	8	9	10
2.6	1	2	3	4	5	7	6	8	9	10
2.7	1	2	3	5	4	7	6	8	9	10
2.8	1	2	3	6	4	7	5	8	9	10
2.9	1	2	3	6	4	7	5	8	9	10
3.0	1	2	3	6	4	7	5	8	9	10

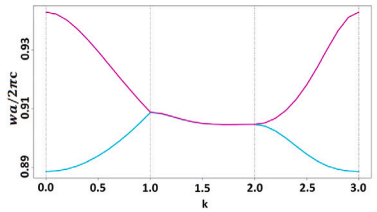

(a) Isolated pair 7 of degree 1 with separated bands 13 and 14

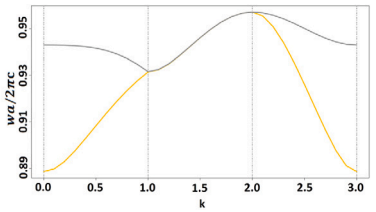

(b) Isolated pair 8 of degree 1 with separated bands 15 and 16

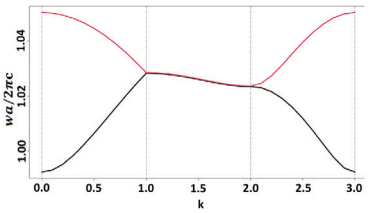

(c) Isolated pair 9 of degree 1 with separated bands 17 and 18

Fig. 19. Separated bands of pairs 7, 8, 9.

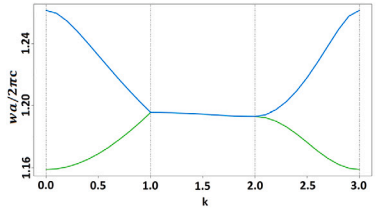

(a) Isolated pair 10 of degree 1 with separated bands 19 and 20

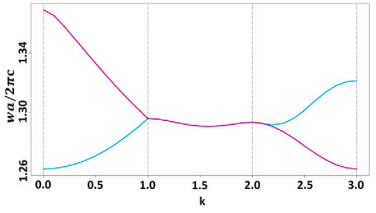

(b) Isolated pair 11 of degree 4 with separated bands 21 and 22

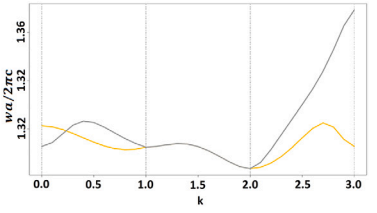

(c) Isolated pair 12 of degree 4 with separated bands 23 and 24

Fig. 20. Separated bands of pairs 10, 11, 12.

When two consecutive pairs are not independent and need to join to obtain a closed loop, we will say that the pair is of superior order 2,3,..., according to the number of bands involved. See for example Fig. 22. Pairs 7 and 8 are of order 2; they require joining two bands in the path $CB'BC'$ to complete a closed loop.

Pair 11 and 12 is an example of a duet of order 4, a closed loop is obtained by joining the points $AC'CD'DB'BA'$ (see Fig. 23).

Table 5
Separation of bands in terms of the original colored bands of COMSOL. Bands 11 to 20.

k	B_{11}	B_{12}	B_{13}	B_{14}	B_{15}	B_{16}	B_{17}	B_{18}	B_{19}	B_{20}
0.0	11	12	13	15	14	16	17	18	19	20
0.1	11	12	13	15	14	16	17	18	19	20
0.2	11	12	13	15	14	16	17	18	19	20
0.3	11	12	13	15	14	16	17	18	19	20
0.4	11	12	13	15	14	16	17	18	19	20
0.5	11	12	13	15	14	16	17	18	19	20
0.6	11	12	13	15	14	16	17	18	19	20
0.7	11	12	13	15	14	16	17	18	19	20
0.8	11	12	13	14	15	16	17	18	19	20
0.9	11	12	13	14	15	16	17	18	19	20
1.0	11	12	13	14	15	16	17	18	19	20
1.1	11	12	13	14	15	16	17	18	19	20
1.2	11	12	13	14	15	16	17	18	19	20
1.3	11	12	13	14	15	16	17	18	19	20
1.4	11	12	13	14	15	16	17	18	19	20
1.5	11	12	13	14	15	16	17	18	19	20
1.6	11	12	13	14	15	16	17	18	19	20
1.7	11	12	13	14	15	16	17	18	19	20
1.8	11	12	13	14	15	16	17	18	19	20
1.9	11	12	13	14	15	16	17	18	19	20
2.0	11	12	13	14	15	16	17	18	19	20
2.1	11	12	13	14	15	16	17	18	19	20
2.2	11	12	13	14	15	16	17	18	19	20
2.3	11	12	13	14	15	16	17	18	19	20
2.4	11	12	13	14	15	16	17	18	19	20
2.5	11	12	13	14	15	16	17	18	19	20
2.6	11	12	13	15	14	16	17	18	19	20
2.7	11	12	13	15	14	16	17	18	19	20
2.8	11	12	13	15	14	16	17	18	19	20
2.9	11	12	13	15	14	16	17	18	19	20
3.0	11	12	13	15	14	16	17	18	19	20

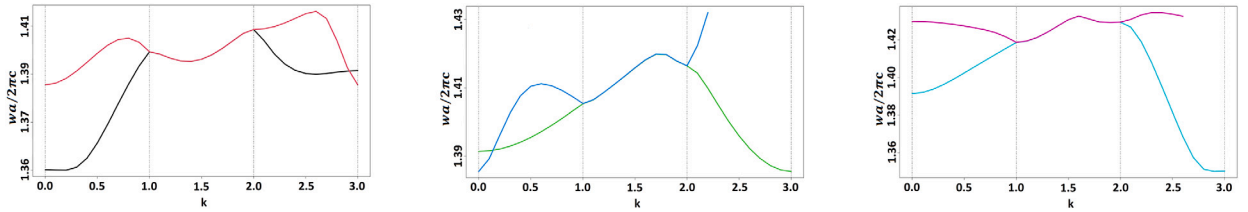

(a) Isolated pair 13 of degree 1 with separated bands 25 and 26

(b) Isolated pair 14 with separated bands 27 and 28

(c) Isolated pair 15 with separated bands 29 and 30

Fig. 21. Separated bands of pairs 13, 14, 15.

3. Conclusions and future work

In this paper we have studied the bands of a square Bravais-Moiré in terms of a remarkable behavior in the second Brilloiun zone, parameterized by $1.0 \leq k \leq 2.0$. All the bands are parallel and very near in the addressed zone. It allows an accurate prediction of the field of the upper band from the electric field of the corresponding lower band. In order to explore the remaining two Brillouin zones ($0.0 \leq k \leq 1.0$, $2.0 \leq k \leq 3.0$), we localize and research an interesting floating pair of bands immersed into a wide band gap modeled by the radio of the scatters. By using an invariant scoring function in certain quotient space, the modeling can be set in terms of the RD. Thus, after learning the behavior of the floating bands, then the remaining crossing pairs can be studied in the elusive Brillouin zones. And with a smooth criterion based on such distance, all the bands of the dispersion can be separated. The order of each pair is also defined in terms of the required bands for obtaining a close loop. The method of this paper has been focus on the square Bravais-Moiré of parameters $r = 2$, $s = 1$, but it has been verified in a number of systems given in [17] and [18]. The mathematical proof via group theory is far to be proposed, but the numerical invariant procedure based on the RD is sufficient for applications. In fact, the provided separated bands are now used in the design of a PC suitable for sensor biochemical substances. The extension of the method for three or more rotated layers of [16] and other related Bravais-Moiré is also studied by the authors. Moreover the search for an atomic crystal material with such remarkable property opens an interesting perspective for applications in electronics and magnetism. Until now, it seems that there is not a natural or artificial material with a similar dispersion relation with parallel bands, however, the task for the corresponding DFT methods just starts, and it is an important open problem to be researched.

Table 6
Separation of bands in terms of the original colored bands of COMSOL. Bands 21 to 30.

k	B_{21}	B_{22}	B_{23}	B_{24}	B_{25}	B_{26}	B_{27}	B_{28}	B_{29}	B_{30}
0.0	21	25	23	22	24	26	28	27	29	30
0.1	21	25	23	22	24	26	28	27	29	30
0.2	21	25	23	22	24	26	27	29	28	30
0.3	21	24	22	23	25	26	27	29	28	30
0.4	21	24	22	23	25	27	26	29	28	30
0.5	21	24	22	23	25	27	26	29	28	30
0.6	21	24	22	23	25	27	26	29	28	30
0.7	21	23	22	24	25	27	26	29	28	30
0.8	21	22	23	24	25	27	26	28	29	30
0.9	21	22	23	24	25	27	26	28	29	30
1.0	21	22	23	24	25	26	27	28	29	30
1.1	21	22	23	24	25	26	27	28	29	30
1.2	21	22	23	24	25	26	27	28	29	30
1.3	21	22	23	24	25	26	27	28	29	30
1.4	21	22	23	24	25	26	27	28	29	30
1.5	21	22	23	24	25	26	27	28	29	30
1.6	21	22	23	24	25	26	27	28	29	30
1.7	21	22	23	24	25	26	27	28	29	30
1.8	21	22	23	24	25	26	27	28	29	30
1.9	21	22	23	24	25	26	27	28	29	30
2.0	21	22	23	24	25	26	27	28	29	30
2.1	21	22	23	24	25	26	27	28	29	30
2.2	22	21	23	24	25	26	27	29	28	30
2.3	22	21	23	24	25	28	26		27	30
2.4	22	21	23	24	25	28	27		26	30
2.5	22	21	23	24	26	28	27		25	30
2.6	22	21	23	24	26	29	27		25	30
2.7	22	21	23	24	27	29	26		25	
2.8	22	21	23	25	27	29	26		24	
2.9	23	21	22	25	27	28	26		24	
3.0	23	21	22	25	28	27	26		24	

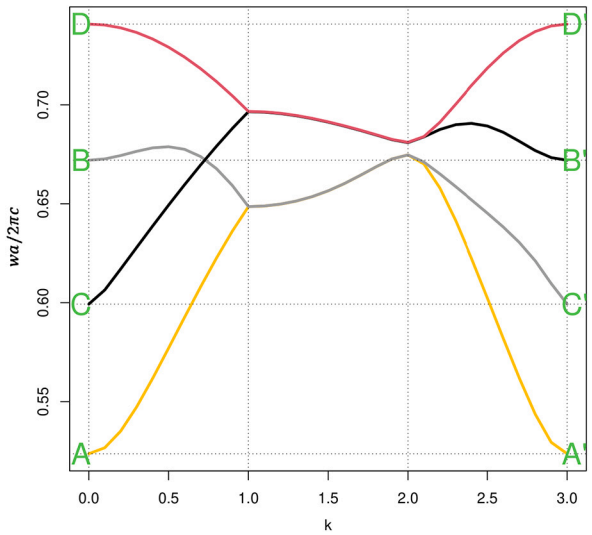

Fig. 22. The double pair 7 and 8 of order 1. The path $CB'BC'$ completes a closed loop.

Unlike their three-dimensional equivalents, planar structure growth enables us to clarify, using models similar to ours, the dynamics of electronic interactions and photonic characteristics. This approach facilitates understanding the selective formation of chiral superlattices, as demonstrated in the patent [43]. Additionally, an intriguing application like Thouless light pumping is advanced through two-dimensional photonic moiré lattices. These are crafted from the Pythagorean moiré design, which combines two square sublattices in a manner akin to our method [44].

Works like ours offer a two-dimensional perspective of the TM-polarized field, characterized and predicted by absorption as an alternative study approach. We introduce a quantification of the electric field modeled from obtaining "constants" related to frequency increase through the tuning of scatterers by varying a scaling factor for the radius. This constant factor could open an

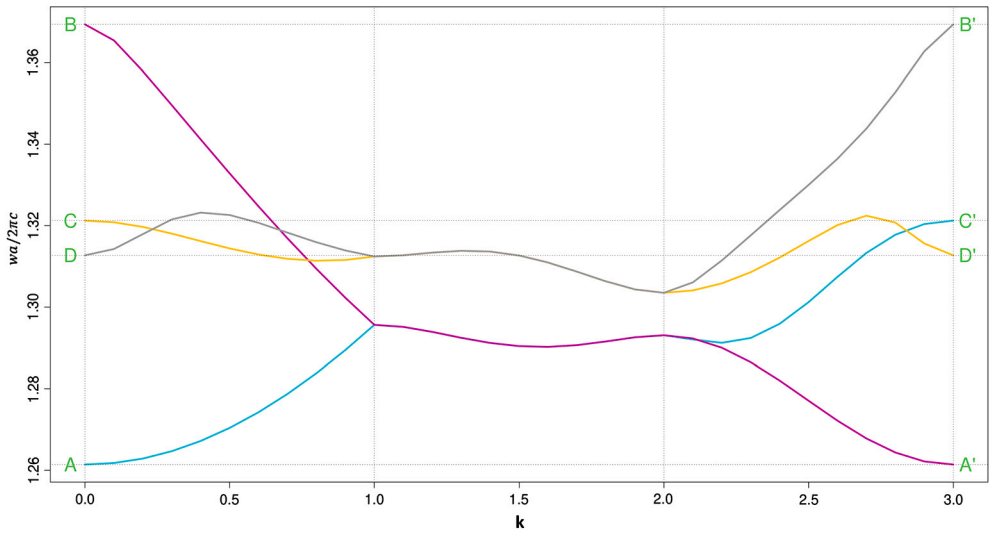

Fig. 23. The double pair 11 and 12 of order 4. The intricate path $AC'CD'DB'BA'$ is required for completing a closed loop.

exciting window for developing Photonic Quantum Computers (PQC) infrastructure. Namely, band separation can be seen as a noise control technique in photon entanglement.

Thus, the commensurability of multiple layers can serve as a mechanism to create photonic crystals with compressible cascading structures featuring unidirectional absorption and promising properties from this enhancement. This approach could offer an alternative for creating Janus Multi-structures used in logic gates and sensing functionalities [45], [46], [47].

CRediT authorship contribution statement

J. Bareño-Silva: Conceptualization, Data curation, Investigation, Writing – original draft. **Á.H. Bedoya-Calle:** Conceptualization, Data curation, Funding acquisition, Resources, Supervision, Visualization, Writing – original draft, Writing – review & editing, Investigation. **H.A. Gómez-Urrea:** Conceptualization, Investigation, Resources, Supervision. **F.J. Caro-Lopera:** Conceptualization, Data curation, Formal analysis, Investigation, Methodology, Resources, Software, Supervision, Validation, Visualization, Writing – original draft.

Declaration of competing interest

The authors declare no competing financial interests or personal relationships that could appear to influence the work reported in this paper.

Data availability

You can access to data associated with this work through the public repository at https://data.mendeley.com/ using the accession number:

https://data.mendeley.com/drafts/7g5ybdxb4k.

Please cite this dataset as follows:

Jose Bareño Silva, Alvaro Bedoya-Calle, Hernan Alejandro Gomez-Urrea, Francisco J. Caro-Lopera, Band separation and electric field prediction in square Bravais-Moiré photonic crystals, (2024), Mendeley Data, V2, DOI: https://doi.org/10.17632/7g5ybdxb4k.2.

Acknowledgement

The authors thank the Faculty of Basic Sciences of the University of Medellin.

Funding. This study was supported by Faculty of Basic Sciences from the University of Medellin.

Appendix A. Supplementary material

Supplementary material related to this article can be found online at https://doi.org/10.1016/j.heliyon.2024.e28275.

References

[1] Alex Figotin, Yuri A. Godin, Ilia Vitebsky, Two-dimensional tunable photonic crystals, Phys. Rev. B 57 (5) (1998) 2841–2848.
[2] Chul-Sik Kee, H. Lim, Tunable complete photonic band gaps of two-dimensional photonic crystals with intrinsic semiconductor rods, Phys. Rev. B 64 (2001) 103–121.
[3] E. Yablonovitch, Inhibited spontaneous emission in solid-state physics and electronics, Phys. Rev. Lett. 58 (20) (1987) 2059–2062.
[4] S. John, Strong localization of photons in certain disordered dielectric superlattices, Phys. Rev. Lett. 58 (23) (1987) 2486–2489.
[5] L. Wu, F. Zhuang, S. He, Degeneracy analysis for a supercell of a photonic crystal and its application to the creation of band gaps, Phys. Rev. E 67 (2) (2003) 026612.
[6] J.J. Jorgensen, J.E. Christensen, T.J. Jarvis, G.L. Hart, A simple, general algorithm for calculating the irreducible Brillouin zone, arXiv preprint arXiv:2104.05856, 2021.
[7] S.A. El-Naggar, H.A. Elsayed, A.H. Aly, Maximization of photonic bandgaps in two-dimensional superconductor photonic crystals, J. Supercond. Nov. Magn. 27 (7) (2014) 1615–1621.
[8] Guida Geraldine, Alain Priou, An introduction to photonic band gap (PBG) materials, Prog. Electromagn. Res. 41 (2003) 1–20.
[9] T. Kariyado, A. Vishwanath, Flat band in twisted bilayer Bravais lattices, Phys. Rev. Res. 1 (3) (2019) 033076.
[10] A. Umenyi, K. Miura, O. Hanaizumi, Modified finite-difference time-domain method for triangular lattice photonic crystals, J. Lightwave Technol. 27 (2009) 22.
[11] Y. Cao, V. Fatemi, S. Fang, et al., Unconventional superconductivity in magic-angle graphene superlattices, Nature 556 (2018) 43–50, https://doi.org/10.1038/nature26160.
[12] S. Shallcross, S. Sharma, E. Kandelaki, O.A. Pankratov, Electronic structure of turbostratic graphene, Phys. Rev. B, Condens. Matter Mater. Phys. 81 (16) (2010) 165105.
[13] S. Shallcross, S. Sharma, O.A. Pankratov, Document quantum interference at the twist boundary in graphene, Phys. Rev. Lett. 101 (5) (2008) 056803.
[14] S. Shallcross, S. Sharma, O.A. Pankratov, Erratum: electronic structure of turbostratic graphene, Phys. Rev. B, Condens. Matter Mater. Phys. 81 (2010) 165105.
[15] Kariyado Toshikaze, Ashvin Vishwanath, Flat band in twisted bilayer Bravais lattices, Phys. Rev. Res. 1 (3) (Nov 2019), https://doi.org/10.1103/physrevresearch.1.033076, American Physical Society (APS).
[16] Francisco J. Caro-Lopera, Bravais-Moiré theory, Technical report, University of Medellin, 2013.
[17] H.A. Gómez-Urrea, M.C. Ospina-Medina, J.D. Correa-Abad, M.E. Mora-Ramosa, F.J. Caro-Lopera, Tunable band structure in 2D Bravais-Moiré photonic crystal lattices, Opt. Commun. 459 (15) (2020) 125081.
[18] H.A. Gómez-Urrea, J. Bareño-Silva, F.J. Caro-Lopera, M.E. Mora-Ramos, The influence of shape and orientation of scatters on the photonic band gap in two-dimensional Bravais-Moiré lattices, Photonics Nanostruct. Fundam. Appl. 42 (2020) 100845.
[19] A. Tiutiunnyk, C.A. Duque, F.J. Caro-Lopera, M.E. Mora-Ramos, J.D. Correa, Opto-electronic properties of twisted bilayer graphene quantum dots, Physica E, Low-Dimens. Syst. Nanostruct. 112 (2019) 36–48.
[20] A.M. Leon, E.A. Velasquez, F. Caro-Lopera, J. Mejia-Lopez, Tuning magnetic order in CrI3 bilayers via Moiré patterns, Adv. Theory Simul. 5 (4) (2022) 2100307.
[21] N. Myoung, H.C. Park, A. Ramachandran, E. Lidorikis, J.-W. Ryu, Flat-band localization and self-collimation of light in photonic crystals, Sci. Rep. 9 (1) (2019), https://doi.org/10.1038/s41598-019-39471-0.
[22] J.D. Joannopoulos, S.G. Johnson, J.N. Winn, R.D. Meade, Photonic Crystals: Molding the Flow of Light, Princeton University Press, 2008.
[23] C.R. Goodall, K.V. Mardia, Multivariate aspects of shape theory, Ann. Stat. 21 (1993) 848–866.
[24] I. Dryden, K.V. Mardia, Statistical Shape Analysis, Wiley, 1998.
[25] F.J. Caro-Lopera, J.A. Díaz-García, G. González-Farías, Noncentral elliptical configuration density, J. Multivar. Anal. 101 (2010) 32–43.
[26] J.A. Díaz-García, F.J. Caro-Lopera, Estimation of mean form and mean form difference under elliptical laws, Electron. J. Stat. 11 (1) (2017) 2424–2460.
[27] J.A. Díaz-García, F.J. Caro-Lopera, Elliptical affine shape distributions for real normed division algebras, J. Multivar. Anal. 144 (2016) 139–149.
[28] J.A. Díaz-García, F.J. Caro-Lopera, Generalised shape theory via pseudo-Wishart distribution, Sankhya A 75 (PART2) (2013) 253–276.
[29] J.A. Díaz-García, F.J. Caro-Lopera, Statistical theory of shape under elliptical models via QR decomposition, Statistics 48 (2) (2014) 456–472.
[30] J.A. Díaz-García, F.J. Caro-Lopera, Generalised shape theory via SV decomposition I, Metrika 75 (4) (2012) 541–565.
[31] J.A. Díaz-García, F.J. Caro-Lopera, Statistical theory of shape under elliptical models and singular value decompositions, J. Multivar. Anal. 103 (1) (2012) 77–92.
[32] COMSOL Multiphysics, Introduction to COMSOL Multiphysics®, COMSOL Multiphysics, Burlington, MA (Accessed Feb 2023).
[33] F.J. Caro Lopera (Productor), Á.H. Bedoya Calle (Autor), J. Bareño Silva (Autor), H.A. Gómez Urrea (Autor), (2023), Software Bravais-Moiré, Software.
[34] R Core Team, R: A Language and Environment for Statistical Computing, R Foundation for Statistical Computing, Vienna, Austria, 2021, https://www.R-project.org/.
[35] Elkin Arias, Francisco J. Caro-Lopera, Elizabeth Flórez, Jhon Fredy Pérez-Torres, Two novel approaches based on the Thompson theory and shape analysis for determination of equilibrium structures of nanoclusters: Cu8, Ag8 and Ag18 as study cases, J. Phys. Conf. Ser. 1247 (2019), conference 1.
[36] F.J. Caro-Lopera, J.A. Díaz-García, G. González-Farías, Inference in affine shape models under elliptical models, J. Korean Stat. Soc. 43 (1) (2014) 67–77.
[37] Francisco J. Caro-Lopera, A family of formulae for pi, Far East J. Math. Sci. 64 (2) (2012) 157–181.
[38] M. Ospina, Modelos matemáticos para la descripción de patrones de Moiré en redes de Bravais, M.Sc. Thesis. Advisors F. Caro-Lopera and J. Correa-Abad, Faculty of Basic Sciences, University of Medellin, 2017.
[39] J.H. Quintero, A. Mariño, L. Siller, E. Restrepo-Parra, F.J. Caro-Lopera, Rocking curves of gold nitride species prepared by arc pulsed - physical assisted plasma vapor deposition, Surf. Coat. Technol. 309 (15 January 2017) 249–257.
[40] J. Quiroz, UdeMedellin Photonics Software, B.Sc. Thesis. Advisors A. Gómez-Urrea and Caro-Lopera Faculty of Basic Sciences, University of Medellin, 2020.
[41] Germán M. Valencia, Jesús A. Anaya, Ever A. Velásquez, Rubén Ramo, Francisco J. Caro-Lopera, About validation-comparison of burned area products, Remote Sens. 12 (23) (2020) 3972.
[42] A.L. Villarreal-Ríos, A.H. Bedoya-Calle, F.J. Caro-Lopera, U. Ortiz-Méndez, M. García-Méndez, F.O. Pérez-Ramírez, Ultrathin tunable conducting oxide films for near-IR applications: an introduction to spectroscopy shape theory, SN Appl. Sci. 1 (2019) 1553.
[43] M.R. Jones, Z. Cheng, Y. Xing, Assembly of Planar Chiral Superlattices from Achiral Building Blocks, United States Patent Application US20230249966, William Marsh Rice University, Pre-Granted Publication, Feb. 2023.
[44] P. Wang, Q. Fu, R. Peng, Y.V. Kartashov, L. Torner, V.V. Konotop, F. Ye, Two-dimensional Thouless pumping of light in photonic Moiré lattices, Nat. Commun. 13 (1) (Nov. 2022), https://doi.org/10.1038/s41467-022-34394-3 [Online].
[45] J. Sui, R. Dong, S. Liao, Z. Zhao, Y. Wang, H.-F. Zhang, Janus metastructure based on magnetized plasma material with and logic gate and multiple physical quantity detection, Ann. Phys. 535 (3) (Jan. 2023), https://doi.org/10.1002/andp.202200509 [Online].
[46] J. Sui, S. Liao, R. Dong, H.-F. Zhang, A Janus logic gate with sensing function, Ann. Phys. 535 (4) (Mar. 2023), https://doi.org/10.1002/andp.202200661 [Online].
[47] S. Guo, C. Hu, H. Zhang, Unidirectional ultrabroadband and wide-angle absorption in graphene-embedded photonic crystals with the cascading structure comprising the Octonacci sequence, J. Opt. Soc. Am. B 37 (9) (Aug. 2020) 2678, https://doi.org/10.1364/josab.399048 [Online].